Front. Chem. Sci. Eng. 2022, 16(10): 1514−1525
https://doi.org/10.1007/s11705-022-2158-y

RESEARCH ARTICLE

Pd/Fe_3O_4 supported on bio-waste derived cellulosic-carbon as a nanocatalyst for C–C coupling and electrocatalytic application

Vishal Kandathil[1*], Akshay Moolakkil[1*], Pranav Kulkarni[1], Alaap Kumizhi Veetil[1], Manjunatha Kempasiddaiah[1], Sasidhar Balappa Somappa[2], R. Geetha Balakrishna[1], Siddappa A. Patil (✉)[1]

1 Centre for Nano and Material Sciences, Jain University, Jain Global Campus, Bangalore 562112, India
2 Organic Chemistry Section, Chemical Sciences & Technology Division, National Institute for Interdisciplinary Science and Technology (CSIR), Thiruvananthapuram 695019, India

Abstract The current work describes the synthesis of a new bio-waste derived cellulosic-carbon supported-palladium nanoparticles enriched magnetic nanocatalyst (Pd/Fe_3O_4@C) using a simple multi-step process under aerobic conditions. Under mild reaction conditions, the Pd/Fe_3O_4@C magnetic nanocatalyst demonstrated excellent catalytic activity in the Hiyama cross-coupling reaction for a variety of substrates. Also, the Pd/Fe_3O_4@C magnetic nanocatalyst exhibited excellent catalytic activity up to five recycles without significant catalytic activity loss in the Hiyama cross-coupling reaction. Also, we explored the use of Pd/Fe_3O_4@C magnetic nanocatalyst as an electrocatalyst for hydrogen evolution reaction. Interestingly, the Pd/Fe_3O_4@C magnetic nanocatalyst exhibited better electrochemical activity compared to bare carbon and magnetite (Fe_3O_4 nanoparticles) with an overpotential of 293 mV at a current density of 10 $mA \cdot cm^{-2}$.

Keywords bio-waste, cellulosic-carbon, Pd/Fe_3O_4, Hiyama cross-coupling, hydrogen evolution reaction, recyclability

1 Introduction

Wherever feasible, the bulk of innovation and technology is currently attempting to shift towards a green and sustainable approach [1]. Because of growing awareness of environmental damage, there has been a surge in interest in creating new approaches to chemical synthesis and processing that reduce energy use while also minimizing emissions [2,3]. Among the approaches to implementing green chemistry principles, heterogeneous catalysis can play a vital role in chemical synthesis [4,5]. The ease of recovering and recycling makes the heterogeneous catalytic systems more cost-efficient and environmentally friendly [6–8]. Carbon is a major support that is used as a heterogeneous support for a wide range of catalyst systems because of its excellent stability, surface area, porous structure and availability [9–11].

Biomass is a huge source of carbon in nature [12]. A lot of agricultural residues are usually burnt in the fields, which results in environmental pollution and are wasted without being used [13]. Only a small portion of this biomass is converted into value-added products [14,15]. The major component of bio-mass is cellulose, which is a bio-polymer [16,17]. Some of the characteristics of cellulose are biodegradability, ease of availability, non-toxicity, cost effectiveness, and eco-friendliness [18,19]. Cellulose and the carbon generated from it have been successfully used in a range of materials science applications, including heterogeneous catalysis, where the availability of hydroxyl groups on cellulose can promote chemical and surface modification [20,21]. The carbon generated from cellulose is often fibrous, has a high purity, and is thermally and chemically stable [22]. A banana pseudostem is a false stem made up of folded leaf blades and sheaths that encircle the growth point and can be used as a source of cellulosic biomass [23]. Cellulose is the main constituent apart from hemicelluloses, pectin, and lignin [23].

The future of catalysis lies in the innovative design and development of unique, highly active, and recyclable nanocomposite catalysts, which will pave the way for green and sustainable technologies to emerge. Carbon as

Received October 23, 2021; accepted January 12, 2022

E-mails: p.siddappa@jainuniversity.ac.in, patilsiddappa@gmail.com

* These authors contributed equally to this work.

a heterogeneous support has certain limitations, particularly in terms of recovering the catalyst from the reaction mass. The inclusion of magnetic nanoparticles into the carbon support improves the catalyst's ease and efficiency of recovery, which in turn increases the number of recycles [20]. The increased number of recycles is beneficial, particularly when the heterogeneous catalyst's active site is a noble metal, which will have a direct impact on process cost. Pd is one of the most studied transition metals because it catalyzes the synthesis of a wide range of C–C coupling reactions, in addition to being an effective hydrogenation catalyst [24–26]. Cross-couplings and related reactions, such as the Hiyama cross-coupling and the Suzuki–Miyaura cross-coupling, are extremely beneficial in the synthesis of numerous essential chemicals [27–29]. However, a transition metal catalyst is required for any of these to proceed at a reasonable rate. Although other metal centers are capable of catalyzing the various steps of these reactions in principle, there is little doubt that Pd catalysts dominate the scene, to the point where, in addition to their synthetic application on a laboratory and industrial scale, these reactions have also become standard procedures for evaluating the reactivity of Pd species as possible catalysts [30].

The Pd catalyzed Hiyama cross-coupling reaction has proven to be an effective approach for generating new C–C bonds with high chemo- and region-selectivity [27]. The Hiyama cross-coupling reaction involves the Pd-catalyzed cross-coupling of organo-silanes activated in the presence of fluoride ions with organic halides, and was promoted as an efficient method of cross-coupling without the use of ultra-reactive (organo-magnesium), toxic (organo-tin), or moisture-sensitive (organo-zinc) main group organometallic compounds. Because of the low polarity of the C–Si bond, organosilicon reagents are inert to standard Pd-catalyzed conditions, unlike other reagents. Nucleophilic fluoride sources, such as tris(dimethylamino)sulfonium difluorotrimethylsilicate [31], tetra-*n*-butylammonium fluoride [32], and, in rare circumstances, KF [33], and CsF [34], were found to be the most popular additives for Hiyama cross-coupling. Some of the drawbacks to employing fluoride activation include the cost and corrosiveness of fluoride ion sources, as well as their incompatibility with common protective groups. Several fluoride-free approaches based on alternate activators or organosilicon reagents have been reported, strengthening the scientific community's acceptance of Hiyama cross-coupling among other C–C bond forming reactions [35].

Hydrogen production is considered as one of the most essential prerequisites for the hydrogen economy. In this context, the hydrogen evolution reaction (HER) provides an effortless and effective solution to the hydrogen economy. Pt is considered as the best electrocatalyst for HER due to its excellent activity and current density, but the limited source and high cost constrain its further development. As an alternative to Pt, Pd remains the best choice according to the volcano plot and is more effective and cheaper catalyst when compared to Pt. Considering the high cost of Pd and to enhance the electroactivity, numerous support materials have been investigated which show improved electronic conductivity and surface area. Li et al. [36] reported Pd coated MoS_2 nanoflowers as an efficient heterostructure catalyst for HER. Numerous strategies have been developed to produce highly electrocatalytically active Pd-based catalysts, but the cost-effectiveness of the system has been one of the major concerns. In this regard, deposition of a small amount of nanosized Pd on a suitable support catalyst could be an effective approach to develop a cost-effective catalyst. The use of various carbon-based support materials such as carbon black, carbon nanotubes, graphene, carbon fiber and Vulcan XC-72 have been successfully used to improve charge transfer and conductivity [37–41]. A limited amount of work has been done on utilizing metal oxides as a support for electrocatalytic HER.

Herein, we report the utilization of bio-waste derived cellulosic-carbon supported-palladium nanoparticles (PdNPs) enriched magnetic nanocatalyst (Pd/Fe_3O_4@C) using a simple multi-step process under aerobic conditions and its efficient utilization in Hiyama cross-coupling reaction and electrochemical HER. The Fe_3O_4@C composite serves as an efficient support for the catalyst which can provide a large surface area and can be magnetically separated and recycled.

2 Experimental

2.1 Materials

All the reactions were carried out in oven-dried glassware with magnetic stirring under aerobic conditions. $FeCl_3 \cdot 6H_2O$ (99%), $FeCl_2 \cdot 4H_2O$ (99%), K_2CO_3 (99%), NH_4OH (~25%), palladium acetate ($Pd(OAc)_2$, 99.98%), Na_2CO_3 (99%), Cs_2CO_3 (99%), KF (98%), NaOH (97%), KOH (97%), aryl halides, trimethoxyphenylsilane ($(CH_3O)_3SiC_6H_5$, 97%), and nafion (≥ 90%) were purchased from Sigma-Aldrich and Avra chemical company which were used without further purification. Banana waste pseudostem (Musa acuminata, Musaceae family) was gathered from local farmers in Yeduvanahalli, Ramanagaram district, Karnataka, India. A silicone oil bath was used to heat the reaction mass. Thin-layer chromatography (TLC) on 0.25 mm Merck TLC silica gel plates with ultra-violet light as a visualizing agent was used to monitor reactions. Flash column chromatography using silica gel 60 (230–400 mesh) was used to purify reaction products. Yields refer to material that is

chromatographically pure. The elimination of volatile solvent with a rotary evaporator equipped with a dry diaphragm pump (1333–1999 Pa), followed by pumping to a constant weight with an oil pump (40 Pa), is referred to as concentration in vacuo.

2.2 Characterization

A PerkinElmer Spectrum Two spectrometer was used for Fourier transform infrared spectroscopy. By physisorption of N_2, Brunauer–Emmett–Teller (BET) surface areas were obtained using a Microtrac BELSORPMAX equipment by physisorption of N_2 after degassing the samples at 180 °C for 2 h. A Perkin Elmer Optima 5300 DV inductively coupled plasma optical emission spectrometer (ICP-OES) was used to measure the elemental Pd concentration of Pd/Fe_3O_4@C. Images of transmission electron microscopy (TEM) were taken with a Jeol/JEM 2100 microscope. A JEOL model JSM7100F was used for field emission scanning electron microscopy (FESEM) and energy dispersive X-ray spectroscopy (EDAX). Thermogravimetric (TG) analysis was performed using a PerkinElmer Diamond TG/DTA at a heating rate of 10.0 °C·min^{-1} and a N_2 gas flow rate of 20 mL·min^{-1}. Powder X-ray diffraction (XRD) patterns were obtained using a Rigaku Ultima-IV XRD system. The electrochemical studies and the catalytic properties of the electrode materials were carried out using a 3-electrode setup with catalysts modified glassy carbon (GC) electrode (geometric area 0.0706 cm^2) as a working electrode, a Pt wire (diameter of 1 mm) as a counter electrode and a saturated calomel electrode (SCE) as a reference electrode. The hydrogen evolution properties were investigated using the electrochemical characterization such as the linear sweep voltammetry (LSV) (Wuhan Corrtest Instruments Corp., Ltd.) in the potential range from 0.05 to –0.3 V (*vs.* SCE) at a scan rate of 5 mV·s^{-1} in 0.5 mol·L^{-1} H_2SO_4. Electrochemical impedance spectroscopy (EIS) was carried out in a frequency range of 0.01 to 0.1 MHz with 5 mV amplitude at a bias potential of 0.02 V (*vs.* reversible hydrogen electrode (RHE)) using CHI660D potentiostat (CH Instruments, Austin, Texas). All the potentials reported in this work were converted to the RHE by adding a value of (0.242 + 0.059 × pH) V.

2.3 Isolation of cellulose from waste pseudostem of banana

The delignification process was carried out as per reported procedure [18,20]. Briefly, the air-dried pseudostem of banana was sliced into small pieces (~250 g) and placed in a 1000 mL beaker to fill up to 75% of its volume. The beaker was filled with 800 mL of 8% NaOH solution. The mixture was then heated on a magnetic stirrer with a hot plate at 90 °C for 7 h, and during that time, the colour of the contents turned brown. Following delignification, the pulp material was subsequently filtered through cloth and washed multiple times with water until it attained neutral pH, before drying in an air oven at 80 °C. To make cellulose powder, dry cellulose was powdered.

2.4 Preparation of Fe_3O_4 magnetic nanoparticles

Fe_3O_4 magnetic nanoparticles were prepared by chemical coprecipitation method as per our previous reports [42,43]. Briefly, about 2.35 g of $FeCl_3·6H_2O$ and 0.86 g of $FeCl_2·4H_2O$ were put into a clean round bottom (R.B) flask containing 40 mL of water. The mixture was then maintained in an oil bath at 85 °C for 30 min with magnetic stirring. After 30 min, added 5 mL of NH_4OH to the mixture to get a black solution. The mixture was then maintained at 85 °C for further 30 min under stirring. The reaction mass was then brought to room temperature and the magnetic Fe_3O_4 nanoparticles were separated from the reaction mass using an external magnet, and the contents were rinsed multiple times with distilled water until the washing reached neutral pH. The Fe_3O_4 particles were then dried at 60 °C.

2.5 Preparation of Pd/Fe_3O_4@C magnetic nanocatalyst

Weighed and transferred 100 mg of $Pd(OAc)_2$, 0.25 g Fe_3O_4, and 1 g of cellulose powder into a 100 mL beaker with a magnetic stir bar. To this beaker, added a minimum quantity of ethylene glycol solvent and kept it in an oil bath for one hour under stirring. The reaction mass turned dark, showing the formation of PdNPs. The contents of the beaker were then transferred to a silica crucible and heated at 300 °C for 4 h inside the muffle furnace. It was then allowed to cool to room temperature before being powdered and weighed to obtain the Pd/Fe_3O_4@C magnetic nanocatalyst.

2.6 General procedure for Hiyama cross-coupling reaction

Aryl halide (1 equiv.), organosilane (1.5 equiv.), Na_2CO_3 (3 equiv.), and Pd/Fe_3O_4@C magnetic nanocatalyst (0.2 mol% Pd) were added to a clean round-bottom flask. Ethylene glycol was then added to the reaction mixture. After that, the contents of the round-bottom flask were sonicated for 30 s to make the reactants uniform. The sonicated mixture was then kept in an oil bath at 100 °C under stirring until the reaction was complete, which was monitored using the TLC technique. After the reaction completion, Pd/Fe_3O_4@C magnetic nanocatalyst was separated using an external magnet, washed with methanol and dried and kept for further use. The reaction mass was then passed through a celite bed to remove any suspended particles. Dichloromethane and distilled water were added and the product was extracted in dichloromethane. The organic layer was then dried with sodium

sulphate and then evaporated to get the crude product. All of the cross-coupled products synthesized were known compounds, which were confirmed by comparing them to the TLC of standard products and by ^1H NMR (nuclear magnetic resonance, cf. Electronic Supplementary Material, ESM).

2.7 Electrode preparation

The electrocatalyst ink was prepared using 2 mg of Pd/Fe_3O_4@C magnetic nanocatalyst and dispersed in a mixture of 200 µL isopropanol, 10 µL Nafion solution and ultrasonicated at high frequency for 30 min. The cleaned GC electrodes were casted with 5 µL of the Pd/Fe_3O_4@C magnetic nanocatalyst and dried in oven for few hours. All the electrode materials were casted on the GC electrodes with 3 mm diameters. Prior to modification, the GC electrodes were polished with different particle sizes (1, 0.3, and 0.05 µm) of alumina particles to ensure proper cleaning. Then the electrodes were rinsed with deionized water and further sonicated in ethanol-water mixture for 10 min. All the electrochemical measurements were carried out at room temperature in 0.5 $mol \cdot L^{-1}$ aqueous H_2SO_4 solution as the supporting electrolyte.

3 Results and discussion

3.1 Synthesis of Pd/Fe_3O_4@C magnetic nanocatalyst

A facile multistep synthesis method was used to synthesize the Pd/Fe_3O_4@C magnetic nanocatalyst. Following a previously described base hydrolysis procedure, the cellulose was isolated from the bio-waste pseudostem of the banana plant, which was subjected to carbonization to form the cellulosic-carbon [18]. The added benefits of cellulose include its easy availability, low cost, and biodegradability, as well as the greater stability and purity of the fibrous carbon formed from it. The primary motivation for using magnetite in this catalytic system was to improve the efficiency of recovering the catalyst after the reaction, thereby increasing the recycling. A coprecipitation strategy was used to synthesize magnetite. The graphical representation of the synthetic technique used to make the Pd/Fe_3O_4@C magnetic nanocatalyst is shown in Fig. 1.

Before being mixed with ethylene glycol solvent, cellulose powder, Fe_3O_4, and $Pd(OAc)_2$ were combined in a 1:0.25:0.1 ratio. The polyol process occurs when heated to 100 °C with stirring, resulting in the reduction of Pd^{2+} to Pd^0 nanoparticles [20]. Furthermore, as described by Gu et al. [44,45] recently, there is a possibility that the cellulose present can function as a reducing and stabilising agent, but the reduction process by cellulose may occur in a lesser proportion here due to the presence of excess ethylene glycol. The reduction process can be observed by a shift in colour from brown to black. After a one-hour reduction process, the reaction mass was calcined in a silica crucible at 300 °C for four hours. Cellulose will be aromatized and depolymerized, resulting in the creation of cellulosic-carbon shielding PdNPs as well as Fe_3O_4 during calcination. After grinding the product to make a homogeneous powder of Pd/Fe_3O_4@C magnetic nanocatalyst, it was used for further studies.

3.2 Structural characterization

After the successful preparation of the Pd/Fe_3O_4@C magnetic nanocatalyst, various physico-chemical characterizations were carried out to confirm the structure and properties of the catalyst (Figs. 2 and 3). The Pd/Fe_3O_4@C magnetic nanocatalyst was subjected to FTIR analysis in order to validate the presence of several functional groups. The FTIR spectrum of cellulosic-carbon and the synthesized Pd/Fe_3O_4@C magnetic nanocatalyst are shown in Fig. 2(a). In the cellulosic-carbon FTIR spectrum, the aromatic C=C stretching is responsible for the band at 1592 cm^{-1}. Aromatic C=C is formed through the aromatization of cellulose, as well as its dehydration and ring opening, which occurs at 300 °C. The band at 2927 cm^{-1} shows the aliphatic C–H stretching and the band at 1056 cm^{-1} can be attributed to the C–O–C skeletal vibrations of the pyranose ring. Characteristic bands at 601 and 638 cm^{-1} of Fe–O stretching vibrations can be seen in the FTIR spectrum of the Pd/Fe_3O_4@C magnetic nanocatalyst (Fig. 2(a)). Fe–OH stretching is

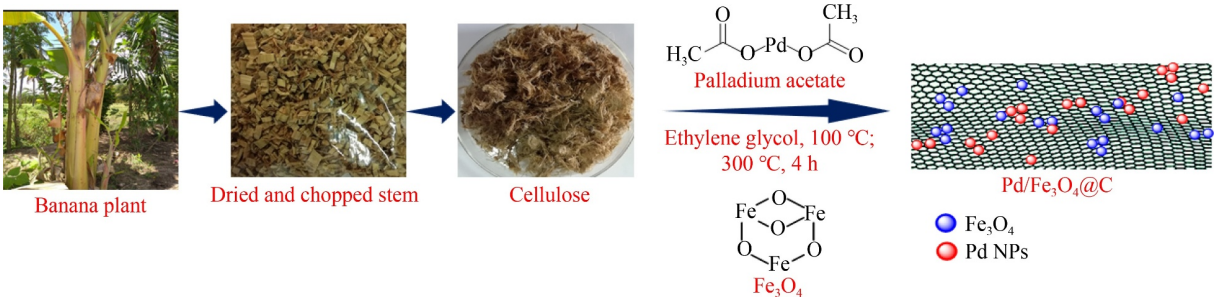

Fig. 1 Schematic representation of synthesis of Pd/Fe_3O_4@C magnetic nanocatalyst.

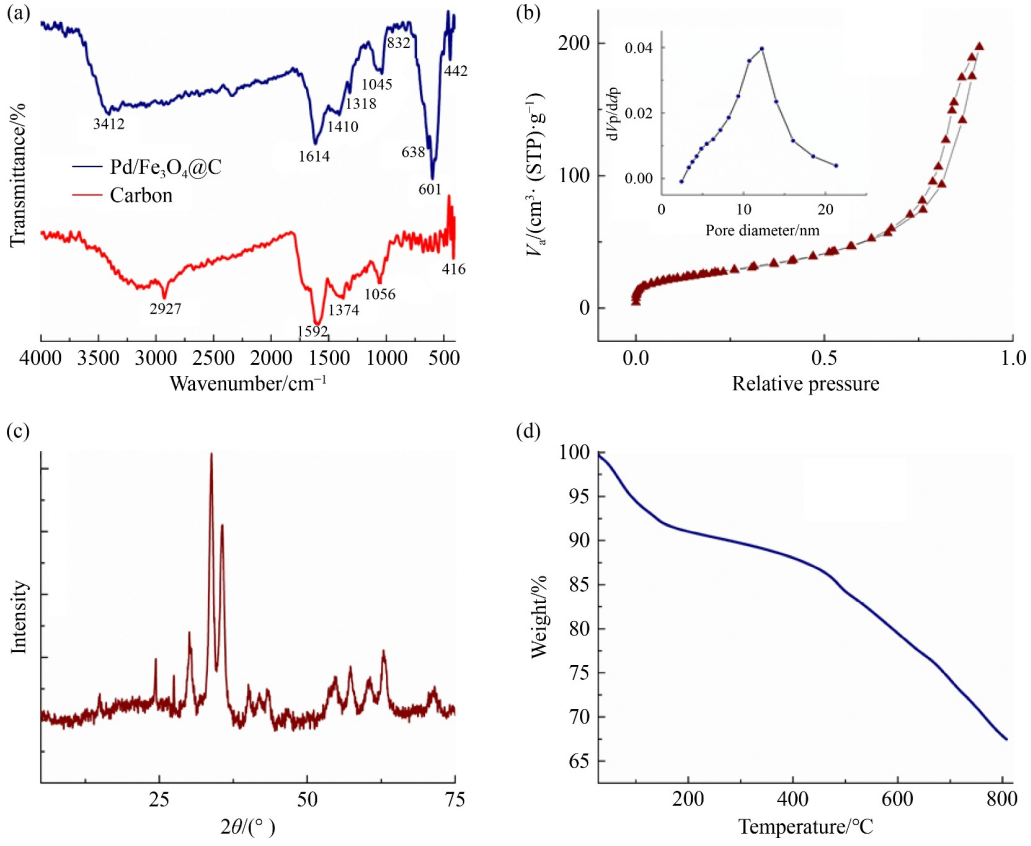

Fig. 2 (a) FTIR spectra of cellulosic-carbon and Pd/Fe_3O_4@C magnetic nanocatalyst; (b) N_2 adsorption–desorption curve and BJH pore size distribution plot (inset) of Pd/Fe_3O_4@C magnetic nanocatalyst; (c) XRD pattern of Pd/Fe_3O_4@C magnetic nanocatalyst; (d) TG curve of Pd/Fe_3O_4@C magnetic nanocatalyst.

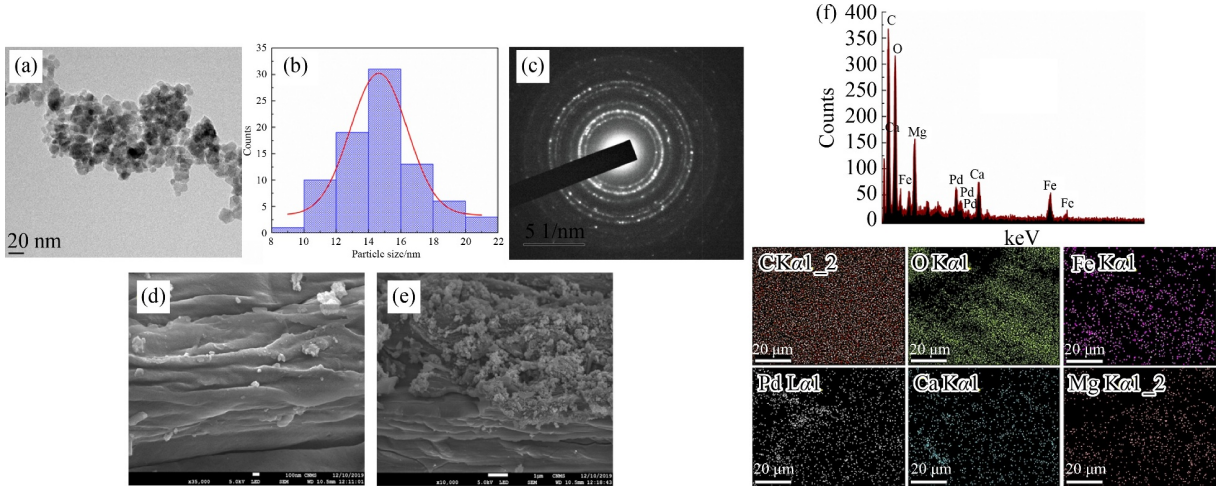

Fig. 3 (a) TEM image, (b) the size distribution histogram and (c) SAED pattern of Pd/Fe_3O_4@C magnetic nanocatalyst; FESEM images of (d) cellulosic-carbon, (e) Pd/Fe_3O_4@C magnetic nanocatalyst and (f) EDAX spectrum and elemental mapping of Pd/Fe_3O_4@C magnetic nanocatalyst.

characterized by the band at 832 cm^{-1}, whereas O–H stretching and bending vibrations are signified by the bands at 3435 and 1318 cm^{-1}. The C–O stretching vibration of the Pd/Fe_3O_4@C magnetic nanocatalyst is observed at 1045 cm^{-1}, while the free C–H bending vibration is observed at 442 cm^{-1}. Furthermore, the bands at 1614 and 1410 cm^{-1}, which match the Pd–C characteristic bands, confirm the formation of a Pd/Fe_3O_4@C magnetic nanocatalyst.

The surface characteristics of the synthesized Pd/Fe_3O_4@C magnetic nanocatalyst were investigated using BET analysis. The N_2 adsorption–desorption isotherm

for the Pd/Fe_3O_4@C magnetic nanocatalyst is shown in Fig. 2(b), and it has a characteristic type-IV isotherm with a tiny hysteresis loop. The Pd/Fe_3O_4@C magnetic nanocatalyst was found to have a BET surface area of 98.4 $m^2 \cdot g^{-1}$. According to the Barrett–Joyner–Halenda (BJH) pore size distribution plot, the pore diameter and pore volume of the Pd/Fe_3O_4@C magnetic nanocatalyst were 12.2 nm and 0.31 $cm^3 \cdot g^{-1}$, respectively (inset of Fig. 2(b)).

The XRD pattern of the Pd/Fe_3O_4@C magnetic nanocatalyst was investigated (Fig. 2(c)). The result indicates a cubic spinel structure with peaks attributed to Fe_3O_4 at 2θ 30.06°, 35.66°, 43.34°, 54.62°, 57.22°, and 62.9° corresponding to reflection planes of (220), (311), (400), (422), (511), and (440) respectively. Three peaks at 2θ 40.04°, 46.5° and 70.46° corresponding to lattice planes (111), (200) and (220) respectively, of PdNPs were also observed, which confirms the face centered cubic crystal structure for PdNPs. Another prominent peak at 33.77° indicates the presence of hematite in the Pd/Fe_3O_4@C magnetic nanocatalyst, which could have formed during the calcination process. Thus, XRD analysis confirms the presence of both Fe_3O_4 and PdNPs. Also, the crystallite size of the Pd/Fe_3O_4@C magnetic nanocatalyst was found to be 11.38 nm by the Scherrer equation.

The thermal stability of the synthesized Pd/Fe_3O_4@C magnetic nanocatalyst was tested using TG analysis, and the TG curve is shown in Fig. 2(d). The elimination of physically adsorbed moisture and solvents, if any, is responsible for the initial weight loss observed up to 150 °C. The breakdown of cellulosic-carbon can cause steady weight loss in the temperature range of 150 to 500 °C. The elimination of the carbonaceous material contained in the Pd/Fe_3O_4@C magnetic nanocatalyst can be linked to a rapid fall in weight percentage from 500 °C onwards.

The morphology and size of the Pd/Fe_3O_4@C magnetic nanocatalyst were investigated using TEM (Fig. 3(a)). The Pd/Fe_3O_4@C magnetic nanocatalyst possesses quasi-spherical nanoparticles dispersed on cellulosic-carbon surfaces, according to TEM images. The average particle size of the Pd/Fe_3O_4@C magnetic nanocatalyst was found to be ~14–15 nm from the size distribution histogram (Fig. 3(b)). The selected area electron diffraction (SAED) pattern exhibits gritty spots in bright field, validating the poly crystalline structure of the Pd/Fe_3O_4@C magnetic nanocatalyst (Fig. 3(c)). Figures 3(d) and 3(e) display FESEM images of cellulosic-carbon from banana pseudostem, and Pd/Fe_3O_4@C magnetic nanocatalyst respectively. The Pd/Fe_3O_4@C magnetic nanocatalyst is made up of homogenous nanometer-sized spherical Pd and Fe_3O_4 particles, whereas the FESEM picture of bare cellulosic-carbon shows fibrous morphology without any nanoparticles dispersed on them. The produced Pd/Fe_3O_4@C magnetic nanocatalyst is highly disseminated and narrowly distributed. The EDAX analysis revealed the presence of all components in the Pd/Fe_3O_4@C magnetic nanocatalyst (Fig. 3(f)) with typical signals of C, O, Fe, and Pd as major elements. We can also confirm that all of the elements are spread nearly evenly using elemental mapping. ICP-OES analysis was used to determine the exact Pd content of the Pd/Fe_3O_4@C magnetic nanocatalyst. The Pd/Fe_3O_4@C magnetic nanocatalyst has a Pd concentration of 27.87% w/w and Fe concentration of 37.22% w/w, according to ICP-OES analysis.

3.3 Catalytic activity study of the Pd/Fe_3O_4@C magnetic nanocatalyst in the Hiyama cross-coupling reaction

After spectroscopic and microscopic structural characterisation of the synthesized Pd/Fe_3O_4@C magnetic nanocatalyst, its catalytic activity as an active and stable magnetically separable nanomagnetic catalyst in the Hiyama cross-coupling reaction was investigated. As illustrated in Scheme 1, the reaction conditions were optimised using a model Hiyama cross-coupling reaction between *p*-iodoanisole and trimethoxyphenylsilane. As indicated in Table 1, the reaction parameters were tuned by a series of reactions. The best yield was obtained using Na_2CO_3 base, ethylene glycol solvent, and 0.2 mol% Pd/Fe_3O_4@C magnetic nanocatalyst at 100 °C (Table 1, entry 12).

To further understand the performance of the Pd/Fe_3O_4@C magnetic nanocatalyst, we explored the role of solvents in the Hiyama cross-coupling process for the model reaction in several solvents such as ethylene glycol, 1,4-dioxane, acetonitrile, and toluene. The results showed that the reaction worked best with the polar protic solvent ethylene glycol, whereas other solvents such as 1,4-dioxane, acetonitrile, and toluene produced lower yields (Table 1, entries 5–7). To better evaluate the performance of the Pd/Fe_3O_4@C magnetic nanocatalyst with different bases on the Hiyama cross-coupling reaction, the model reaction was carried out using various bases such as NaOH, KOH, Na_2CO_3, K_2CO_3, and Cs_2CO_3 (Table 1, entries 9–13). Although all of the bases were shown to be effective, Na_2CO_3 was picked as the optimal base due to its mildness and inexpensiveness when compared to other harsh bases. The reaction temperature

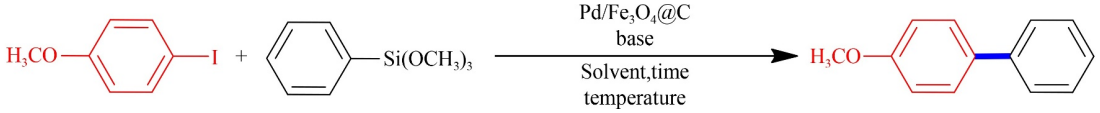

Scheme 1 Hiyama cross-coupling reaction between *p*-iodoanisole and trimethoxyphenylsilane in the presence of Pd/Fe_3O_4@C magnetic nanocatalyst.

Table 1 Optimization of reaction conditions for Hiyama cross-coupling reaction of *p*-iodoanisole with trimethoxyphenylsilane in presence of the Pd/Fe_3O_4@C magnetic nanocatalyst [a)]

Entry	Base	Solvent	Pd/mol%	Temperature/°C	Time/h	Yield/% [b)]
1	NaOH	Ethylene glycol	–	100	1	–
2	NaOH	Ethylene glycol	0.3	100	0.25	90
3	NaOH	Ethylene glycol	0.2	100	0.5	90
4	NaOH	Ethylene glycol	0.1	100	0.5	40
5	NaOH	1,4-Dioxane	0.2	100	0.5	20
6	NaOH	Acetonitrile	0.2	80	0.5	20
7	NaOH	Toluene	0.2	100	0.5	35
8	NaOH	Ethylene glycol	0.2	80	0.5	45
9	NaOH	Ethylene glycol	0.2	120	0.25	92
10	KOH	Ethylene glycol	0.2	100	0.5	80
11	K_2CO_3	Ethylene glycol	0.2	100	0.5	80
12	Na_2CO_3	Ethylene glycol	0.2	100	0.5	90
13	Cs_2CO_3	Ethylene glycol	0.2	100	0.5	85

a) Reaction condition: *p*-iodoanisole (1 equiv.), trimethoxyphenylsilane (1.5 equiv.), base (3 equiv.) and solvent (5 mL) in air; b) isolated yield.

has a significant impact on the Hiyama cross-coupling reaction. At reaction temperatures above 100 °C, a significant conversion rate was found and there was a decrease in the yields at lower reaction temperatures (Table 1, entries 7–9). As a result, the reactions were carried out at a temperature of 100 °C. In the Hiyama cross-coupling reaction, the catalyst quantity plays a crucial role. We conducted the model Hiyama cross-coupling reaction with varied amounts of Pd/Fe_3O_4@C magnetic nanocatalyst, ranging from 0.1 mol% Pd to 0.3 mol% Pd, in order to determine the suitable quantity of Pd/Fe_3O_4@C magnetic nanocatalyst (Table 1, entries 2–4). With 0.2 mol% Pd in the Pd/Fe_3O_4@C magnetic nanocatalyst, a greater conversion rate was achieved.

The Pd/Fe_3O_4@C magnetic nanocatalyst was used in Hiyama cross-coupling for a variety of aryl bromides and aryl iodides using optimized reaction conditions (Scheme 2) and the findings are summarized in Table 2. When aryl halides were substituted with an electron-donating group, the yield was lower than when the electron-withdrawing substituent was used. All of the aryl iodides produced satisfactory to excellent results. Aryl bromides, on the other hand, produced a lower yield, with the exception of bromobenzene and 4-bromotoluene (Table 2, entries 9 and 14). This is due to the fact that iodides are less electronegative than bromides. These findings corroborated our Pd/Fe_3O_4@C magnetic nanocatalyst's excellent performance in the Hiyama cross-coupling reaction.

A comparative catalytic activity study of the Pd/Fe_3O_4@C magnetic nanocatalyst with a previously reported nanocatalyst with an almost similar Pd loading was performed (Table S1, cf. ESM) in the Hiyama cross-coupling reaction [20]. It was found that the catalytic activity of the Pd/Fe_3O_4@C magnetic nanocatalyst in Hiyama cross-coupling was better than that of the Pd-MNP@SCB, which can be attributed to the slightly higher availability of active Pd sites. Further, to understand the advantages of the Pd/Fe_3O_4@C magnetic nanocatalyst in the Hiyama cross-coupling reaction when compared with other reports, we have compared the results and reaction conditions and summarized them in Table S2 (cf. ESM). By the comparison of activities, we can clearly understand that the Pd/Fe_3O_4@C magnetic nanocatalyst has comparable yields at the same time the reaction is completed in less time with comparatively lower catalyst loadings.

3.4 Recyclability study of the Pd/Fe_3O_4@C magnetic nanocatalyst

The model Hiyama cross-coupling reaction was chosen for the recyclability study using Pd/Fe_3O_4@C magnetic nanocatalyst and the result obtained is depicted in Fig. 4. The Pd/Fe_3O_4@C magnetic nanocatalyst was retrieved from the reaction mixture using an external magnet after the reaction was completed, and was utilized in the next run after washing with distilled water, followed by methanol wash and drying. According to the results obtained, the Pd/Fe_3O_4@C magnetic nanocatalyst may be recycled up to five times without losing significant yield. There is a considerable reduction in catalytic activity from the sixth recycle forward. The activity loss can be ascribed to the palladium leaching from the Pd/Fe_3O_4@C

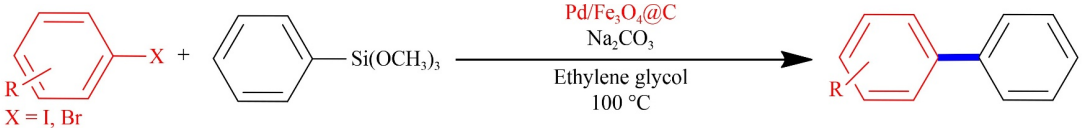

Scheme 2 Hiyama cross-coupling reaction in the presence of Pd/Fe_3O_4@C magnetic nanocatalyst.

Table 2 Hiyama cross-coupling reaction between aryl halides and trimethoxyphenylsilane catalyzed by Pd/Fe_3O_4@C magnetic nanocatalyst [a)]

Entry	Aryl halide	Product	Time/min	Yield/% [b)]
1	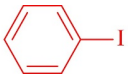	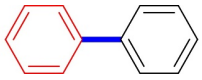	30	95
2	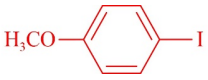	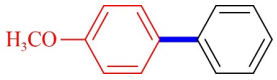	30	90
3		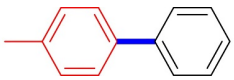	30	90
4	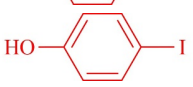	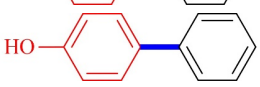	90	70
5	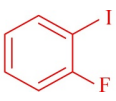	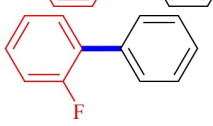	15	92
6	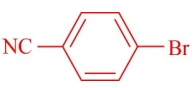	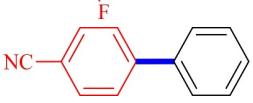	180	80
7	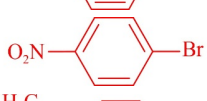	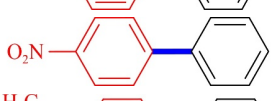	30	85
8	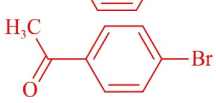	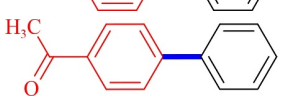	240	50
9		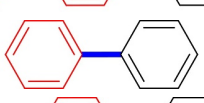	60	95
10	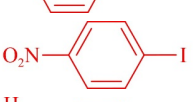	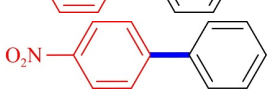	70	98
11	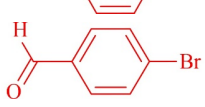	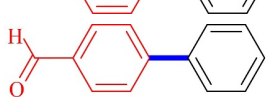	120	70
12	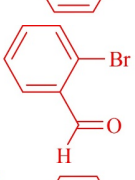	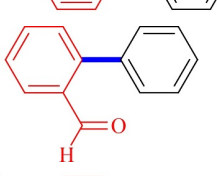	90	50
13	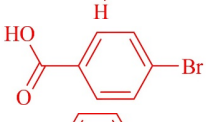	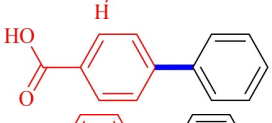	180	50
14	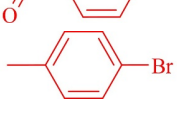	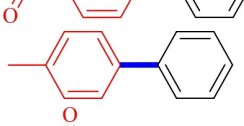	60	92
15	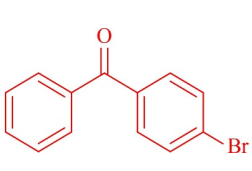	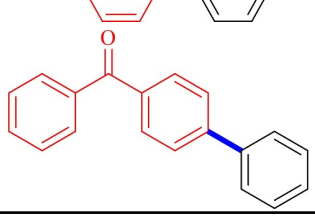	240	70

a) Reaction conditions: aryl halide (1 equiv.), trimethoxyphenylsilane (1.5 equiv.), base (3 equiv.), Pd/Fe_3O_4@C magnetic nanocatalyst (0.2 mol% of Pd with respect to aryl halide) and solvent (5 mL) in air; b) isolated yield.

magnetic nanocatalyst. The Pd/Fe_3O_4@C magnetic nanocatalyst was analyzed using FTIR and FESEM techniques after five recycles to understand the structural and morphological changes that might have happened during the reaction (Fig. 5). The FTIR spectrum of five times recycled Pd/Fe_3O_4@C magnetic nanocatalyst (Fig. 5(a)) indicates there is slow disintegration in the chemical composition of the catalyst when compared with the fresh one. The FESEM images of five times recycled Pd/Fe_3O_4@C magnetic nanocatalyst (Figs. 5(b) and 5(c)) reveal that the morphology of the Pd/Fe_3O_4@C magnetic nanocatalyst does not change significantly even though there is some enhancement in the agglomeration of particles after five recycles.

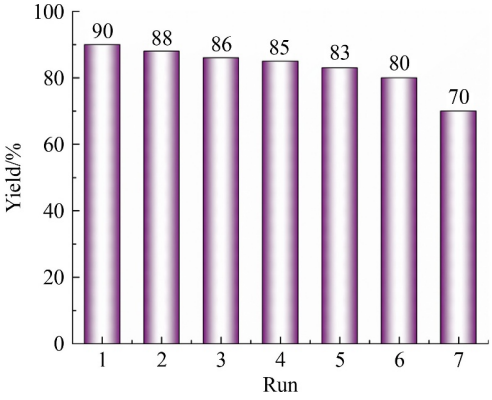

Fig. 4 The recycling efficiency of the Pd/Fe_3O_4@C magnetic nanocatalyst in the model Hiyama cross-coupling reaction.

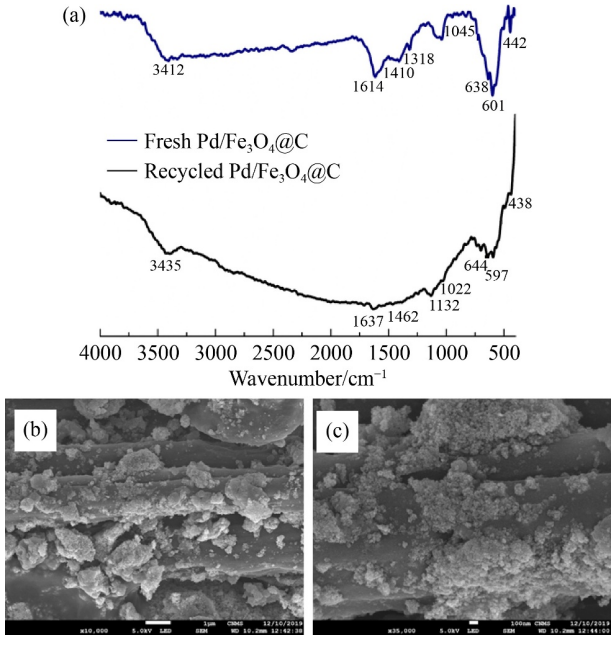

Fig. 5 (a) FT-IR spectra of fresh and five times recycled Pd/Fe_3O_4@C magnetic nanocatalyst; (b, c) FESEM images of Pd/Fe_3O_4@C magnetic nanocatalyst after five recycles.

3.5 Leaching study

A leaching experiment on the model Hiyama cross-coupling reaction was conducted to further demonstrate the heterogeneity of the Pd/Fe_3O_4@C magnetic nanocatalyst. Initially, a calculated quantity of Pd/Fe_3O_4@C magnetic nanocatalyst was added to the solvent system containing the base and agitated at 100 °C for 1 h. The Pd/Fe_3O_4@C magnetic nanocatalyst was subsequently separated and the aryl halide and organosilane were added to the same reaction mass and stirred. The absence of any product formation confirmed by reaction monitoring even after 2 h at optimized reaction conditions proved that the reaction mass did not contain any leached-out palladium. In addition, the ICP-OES analysis was performed on the above reaction mass and the palladium content obtained was $< 0.01 \times 10^{-6}$ which further proves the lack of Pd in this reaction mass. It is therefore possible to conclude that the Pd/Fe_3O_4@C magnetic nanocatalyst is heterogeneous in nature. The abundance of functional groups on the biomass carbon can be attributed to the electrostatic attachment of PdNPs in the Pd/Fe_3O_4@C magnetic nanocatalyst and thereby preventing the leaching out of the active centers.

3.6 Electrocatalytic performance

To evaluate the electrocatalytic activities of the as synthesized Pd/Fe_3O_4@C magnetic nanocatalyst as an electrocatalyst for HER (Fig. 6), LSV was carried out in 0.5 mol·L^{-1} H_2SO_4 at a scan rate of 5 mV·s^{-1}, as shown in Fig. 6(a). For comparison, the contribution of bare carbon and Fe_3O_4 towards HER were studied (inset of Fig. 6(a)). Figure 6(a) shows an overpotential of 229 mV at current density of 5 mA·cm^{-2} and 293 mV at current density of 10 mA·cm^{-2} for Pd/Fe_3O_4@C magnetic nanocatalyst *vs.* RHE. When compared to the Pd/Fe_3O_4@C magnetic nanocatalyst, the current density for bare C and Fe_3O_4@C was relatively low, indicating that the latter had less activity in the HER. The presence of a small amount of Pd in the composite enhanced the electrocatalytic activity. The Tafel slope was calculated from the slope of the overpotential *vs.* logarithmic current density and was found to be 227.05 mV·dec^{-1} for the Pd/Fe_3O_4@C magnetic nanocatalyst (Fig. 6(b)). EIS was carried out to obtain further insights into the catalytic activity as shown in Fig. 6(c). The Nyquist plot shows a large charge transfer of 712 Ω for the bare GC electrode. In the case of bare Fe_3O_4@C support, a charge transfer resistance of 204 Ω was obtained; whereas the Pd/Fe_3O_4@C magnetic nanocatalyst displayed a low charge transfer resistance, which could be attributed to the presence of a trace quantity of PdNPs in the hybrid composite. This improved charge transfer property resulted in better electrocatalytic activity towards HER. A comparison of the electrochemical activity of Pd/Fe_3O_4@C magnetic nanocatalyst with different supports has been tabulated in Table S3 (cf. ESM). From comparison data, it can be understood that palladium-based catalysts generally show high activity towards HER and our catalyst also shows activity which is comparable with other systems.

4 Conclusions

In summary, the carbonized pseudostem of banana and synthesized magnetite nanoparticles were used as a recyclable support for PdNPs in the Hiyama cross-coupling reaction as well as in electrocatalysis, resulting in an efficient and green nanocatalyst. Spectroscopic,

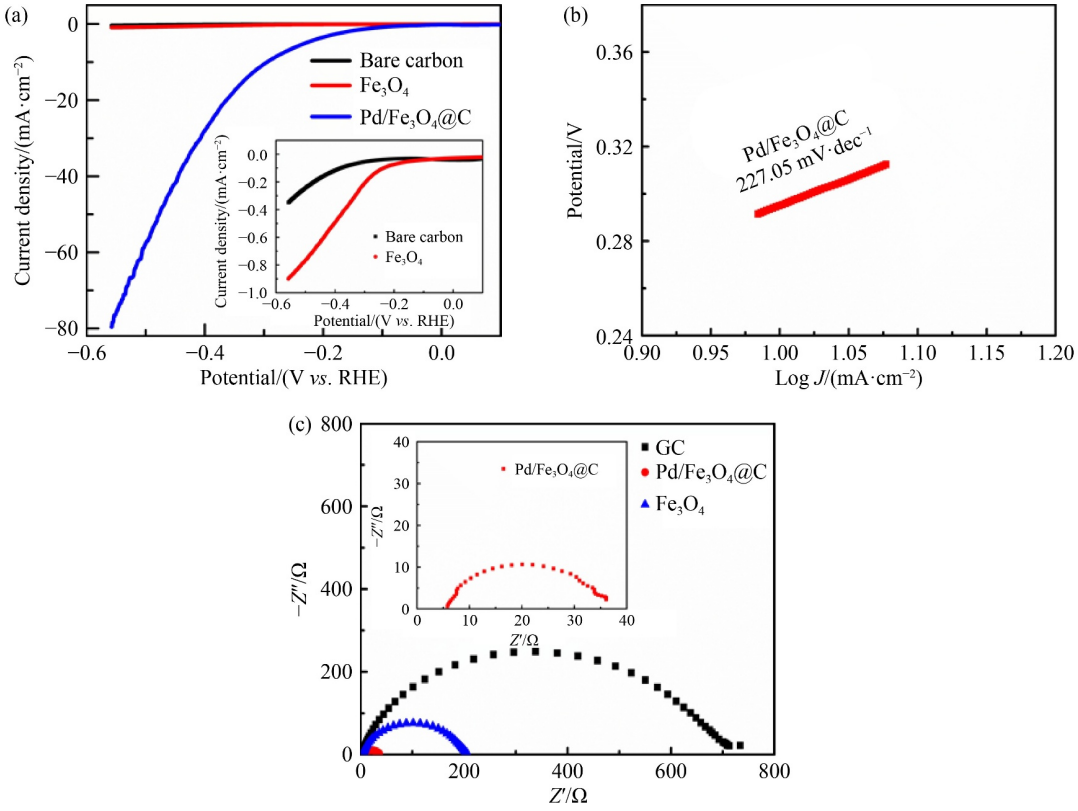

Fig. 6 Electrochemical measurements of the electrocatalyst (a) polarization curves of pure bare carbon, Fe_3O_4 and Pd/Fe_3O_4@C heterostructure. (b) Tafel plots for Pd/Fe_3O_4@C and (c) EIS of glassy carbon, Fe_3O_4 and Pd/Fe_3O_4@C heterostructures.

microscopic, thermal, and surface investigations were carried out to characterize the produced Pd/Fe_3O_4@C magnetic nanocatalyst. The present approach stresses the utilization of waste banana pseudostem as a carbon source, avoiding poisonous and dangerous chemicals as catalyst support. Furthermore, the Hiyama cross-coupling reaction was performed without using any fluoride source. The organic transformation yields were comparable to previously published catalytic systems, and in some cases, outperformed them. The proposed method also has the benefits of green synthesis, ligand-free conditions, and recyclability. Interestingly, the as synthesized Pd/Fe_3O_4@C magnetic nanocatalyst showed an overpotential of 293 mV at 10 $mA \cdot cm^{-2}$ with a Tafel slope of 227.05 $mV \cdot dec^{-1}$, which was better than its counter parts. The Pd/Fe_3O_4@C magnetic nanocatalyst showed lower charge transfer resistance and good electrochemical activity as an electrocatalyst for HER. Thus, the Pd/Fe_3O_4@C magnetic nanocatalyst was successfully investigated for its dual role in the C–C coupling reaction and the HER.

Acknowledgements The authors thank DST-SERB, India (YSS/2015/000010), DST-Nanomission, India (SR/NM/NS-20/2014), and Jain University, India for financial support.

Electronic Supplementary Material Supplementary material is available in the online version of this article at https://dx.doi.org/10.1007/s11705-022-2158-y and is accessible for authorized users.

References

1. García-Serna J, Pérez-Barrigón L, Cocero M. New trends for design towards sustainability in chemical engineering: green engineering. Chemical Engineering Journal, 2007, 133(1-3): 7–30
2. Centi G, Ciambelli P, Perathoner S, Russo P. Environmental catalysis: trends and outlook. Catalysis Today, 2002, 75(1-4): 3–15
3. Clarke C J, Tu W C, Levers O, Brohl A, Hallett J P. Green and sustainable solvents in chemical processes. Chemical Reviews, 2018, 118(2): 747–800
4. Descorme C, Gallezot P, Geantet C, George C. Heterogeneous catalysis: a key tool toward sustainability. ChemCatChem, 2012, 4(12): 1897–1906
5. Di Monte R, Kašpar J. Heterogeneous environmental catalysis—a gentle art: CeO_2–ZrO_2 mixed oxides as a case history. Catalysis Today, 2005, 100(1-2): 27–35
6. Beletskaya I, Tyurin V. Recyclable nanostructured catalytic systems in modern environmentally friendly organic synthesis. Molecules, 2010, 15(7): 4792–4814
7. Polshettiwar V, Varma R S. Green chemistry by nano-catalysis. Green Chemistry, 2010, 12(5): 743–754
8. Beletskaya I P, Kustov L M. Catalysis as an important tool of green chemistry. Russian Chemical Reviews, 2010, 79(6): 441–461
9. Rodriguez-Reinoso F. The role of carbon materials in heterogeneous catalysis. Carbon, 1998, 36(3): 159–175

10. Antolini E. Carbon supports for low-temperature fuel cell catalysts. Applied Catalysis B: Environmental, 2009, 88(1-2): 1–24
11. Julkapli N M, Bagheri S. Graphene supported heterogeneous catalysts: an overview. International Journal of Hydrogen Energy, 2015, 40(2): 948–979
12. Houghton R, Hall F, Goetz S J. Importance of biomass in the global carbon cycle. Journal of Geophysical Research. Biogeosciences, 2009, 114(G2): 1–13
13. Bhuvaneshwari S, Hettiarachchi H, Meegoda J N. Crop residue burning in India: policy challenges and potential solutions. International Journal of Environmental Research and Public Health, 2019, 16(5): 832
14. Lim J S, Manan Z A, Alwi S R W, Hashim H. A review on utilisation of biomass from rice industry as a source of renewable energy. Renewable & Sustainable Energy Reviews, 2012, 16(5): 3084–3094
15. Singh R, Srivastava M, Shukla A. Environmental sustainability of bioethanol production from rice straw in India: a review. Renewable & Sustainable Energy Reviews, 2016, 54: 202–216
16. Quignard F, Choplin A. Cellulose: a new bio-support for aqueous phase catalysts. Chemical Communications, 2001(1): 21–22
17. Sekhar C P, Kalidhasan S, Rajesh V, Rajesh N. Bio-polymer adsorbent for the removal of malachite green from aqueous solution. Chemosphere, 2009, 77(6): 842–847
18. Kandathil V, Kempasiddaiah M, Sasidhar B, Patil S A. From agriculture residue to catalyst support; a green and sustainable cellulose-based dip catalyst for CC coupling and direct arylation. Carbohydrate Polymers, 2019, 223: 115060
19. Moon R J, Martini A, Nairn J, Simonsen J, Youngblood J. Cellulose nanomaterials review: structure, properties and nanocomposites. Chemical Society Reviews, 2011, 40(7): 3941–3994
20. Kandathil V, Veetil A K, Patra A, Moolakkil A, Kempasiddaiah M, Somappa S B, Rout C S, Patil S A. A green and sustainable cellulosic-carbon-shielded Pd-MNP hybrid material for catalysis and energy storage applications. Journal of Nanostructure in Chemistry, 2021, 11(3): 395–407
21. Zhang Y, Hao N, Lin X, Nie S. Emerging challenges in the thermal management of cellulose nanofibril-based supercapacitors, lithium-ion batteries and solar cells: a review. Carbohydrate Polymers, 2020, 234: 115888
22. Dumanlı A G, Windle A H. Carbon fibres from cellulosic precursors: a review. Journal of Materials Science, 2012, 47(10): 4236–4250
23. Jayaprabha J, Brahmakumar M, Manilal V. Banana pseudostem characterization and its fiber property evaluation on physical and bioextraction. Journal of Natural Fibers, 2011, 8(3): 149–160
24. Astruc D. Palladium nanoparticles as efficient green homogeneous and heterogeneous carbon−carbon coupling precatalysts: a unifying view. Inorganic Chemistry, 2007, 46(6): 1884–1894
25. McCue A J, Anderson J A. Recent advances in selective acetylene hydrogenation using palladium containing catalysts. Frontiers of Chemical Science and Engineering, 2015, 9(2): 142–153
26. Kandathil V, Kulkarni B, Siddiqa A, Kempasiddaiah M, Sasidhar B S, Patil S A. Immobilized *N*-heterocyclic carbene-palladium(II) complex on graphene oxide as efficient and recyclable catalyst for Suzuki−Miyaura cross-coupling and reduction of nitroarenes. Catalysis Letters, 2020, 150(2): 384–403
27. Foubelo F, Nájera C, Yus M. The Hiyama cross-coupling reaction: new discoveries. Chemical Record, 2016, 16(6): 2521–2533
28. Maluenda I, Navarro O. Recent developments in the Suzuki–Miyaura reaction: 2010–2014. Molecules, 2015, 20(5): 7528–7557
29. Kandathil V, Siddiqa A, Patra A, Kulkarni B, Kempasiddaiah M, Sasidhar B S, Patil S A, Rout C S, Patil S A. NHC-Pd complex heterogenized on graphene oxide for cross-coupling reactions and supercapacitor applications. Applied Organometallic Chemistry, 2020, 34(11): e5924
30. Wu X F, Neumann H, Beller M. Synthesis of heterocycles via palladium-catalyzed carbonylations. Chemical Reviews, 2013, 113(1): 1–35
31. Hatanaka Y, Hiyama T. Cross-coupling of organosilanes with organic halides mediated by a palladium catalyst and tris(diethylamino) sulfonium difluorotrimethylsilicate. Journal of Organic Chemistry, 1988, 53(4): 918–920
32. Tamao K, Kobayashi K, Ito Y. Palladium-catalyzed cross-coupling reaction of alkenylalkoxysilanes with aryl and alkenyl halides in the presence of a fluoride ion. Tetrahedron Letters, 1989, 30(44): 6051–6054
33. Ichii S, Hamasaka G, Uozumi Y. The Hiyama cross-coupling reaction at parts per million levels of Pd: *in situ* formation of highly active spirosilicates in glycol solvents. Chemistry, an Asian Journal, 2019, 14(21): 3850–3854
34. Nozawa-Kumada K, Osawa S, Sasaki M, Chataigner I, Shigeno M, Kondo Y. Deprotonative silylation of aromatic C–H bonds mediated by a combination of trifluoromethyltrialkylsilane and fluoride. Journal of Organic Chemistry, 2017, 82(18): 9487–9496
35. Kandathil V, Dateer R B, Sasidhar B, Patil S A, Patil S A. Green synthesis of palladium nanoparticles: applications in aryl halide cyanation and Hiyama cross-coupling reaction under ligand free conditions. Catalysis Letters, 2018, 148(6): 1562–1578
36. Li B, Qiao S, Zheng X, Yang X, Cui Z, Zhu S, Li Z Y, Liang Q Y. Pd coated MoS_2 nanoflowers for highly efficient hydrogen evolution reaction under irradiation. Journal of Power Sources, 2015, 284: 68–76
37. Grigoriev S, Millet P, Fateev V. Evaluation of carbon-supported Pt and Pd nanoparticles for the hydrogen evolution reaction in PEM water electrolysers. Journal of Power Sources, 2008, 177(2): 281–285
38. Grigoriev S, Mamat M, Dzhus K, Walker G, Millet P. Platinum and palladium nano-particles supported by graphitic nano-fibers as catalysts for PEM water electrolysis. International Journal of Hydrogen Energy, 2011, 36(6): 4143–4147
39. Mahesh K N, Balaji R, Dhathathreyan K. Palladium nanoparticles as hydrogen evolution reaction (HER) electrocatalyst in electrochemical methanol reformer. International Journal of Hydrogen Energy, 2016, 41(1): 46–51
40. Ghasemi S, Hosseini S R, Nabipour S, Asen P. Palladium nanoparticles supported on graphene as an efficient electrocatalyst for hydrogen evolution reaction. International

Journal of Hydrogen Energy, 2015, 40(46): 16184–16191

41. Huang Y X, Liu X W, Sun X F, Sheng G P, Zhang Y Y, Yan G M, Wang S G, Xu A W, Yu H Q. A new cathodic electrode deposit with palladium nanoparticles for cost-effective hydrogen production in a microbial electrolysis cell. International Journal of Hydrogen Energy, 2011, 36(4): 2773–2776
42. Vishal K, Fahlman B D, Sasidhar B S, Patil S A, Patil S A. Magnetic nanoparticle-supported *N*-heterocyclic carbene-palladium(II): a convenient, efficient and recyclable catalyst for Suzuki−Miyaura cross-coupling reactions. Catalysis Letters, 2017, 147(4): 900–918
43. Kandathil V, Fahlman B D, Sasidhar B S, Patil S A, Patil S A. A convenient, efficient and reusable *N*-heterocyclic carbene-palladium(II) based catalyst supported on magnetite for Suzuki−Miyaura and Mizoroki−Heck cross-coupling reactions. New Journal of Chemistry, 2017, 41(17): 9531–9545
44. Gu J, Hu C, Zhang W, Dichiara A B. Reagentless preparation of shape memory cellulose nanofibril aerogels decorated with Pd nanoparticles and their application in dye discoloration. Applied Catalysis B: Environmental, 2018, 237: 482–490
45. Gu J, Dichiara A. Hybridization between cellulose nanofibrils and faceted silver nanoparticles used with surface enhanced Raman scattering for trace dye detection. International Journal of Biological Macromolecules, 2020, 143: 85–92